



# Characterization of metallization and amorphization for GaP under different hydrostatic environments in diamond anvil cell up to 40.0 GPa

Cite as: Rev. Sci. Instrum. **90**, 066103 (2019); <https://doi.org/10.1063/1.5093949>

Submitted: 26 February 2019 . Accepted: 29 May 2019 . Published Online: 14 June 2019

Lidong Dai , Chang Pu, Heping Li , Haiying Hu, Kaixiang Liu, Linfei Yang, and Meiling Hong



View Online



Export Citation



CrossMark

## ARTICLES YOU MAY BE INTERESTED IN

[New dynamic diamond anvil cells for tera-pascal per second fast compression x-ray diffraction experiments](#)

Review of Scientific Instruments **90**, 065114 (2019); <https://doi.org/10.1063/1.5098993>

[A fast key parameter extraction algorithm for long fiber distributed sensing based on Brillouin scattering](#)

Review of Scientific Instruments **90**, 066101 (2019); <https://doi.org/10.1063/1.5049738>

[Real-time digital signal recovery for sensors and amplifiers with resonant characteristics](#)

Review of Scientific Instruments **90**, 065109 (2019); <https://doi.org/10.1063/1.5081789>

Lock-in Amplifiers  
up to 600 MHz



# Characterization of metallization and amorphization for GaP under different hydrostatic environments in diamond anvil cell up to 40.0 GPa

Cite as: Rev. Sci. Instrum. 90, 066103 (2019); doi: 10.1063/1.5093949

Submitted: 26 February 2019 • Accepted: 29 May 2019 •

Published Online: 14 June 2019



View Online



Export Citation



CrossMark

Lidong Dai,<sup>1,a)</sup> Chang Pu,<sup>1,2</sup> Heping Li,<sup>1</sup> Haiying Hu,<sup>1</sup> Kaixiang Liu,<sup>1,2</sup> Linfei Yang,<sup>1,2</sup> and Meiling Hong<sup>1,2</sup>

## AFFILIATIONS

<sup>1</sup>Key Laboratory of High Temperature and High Pressure Study of the Earth's Interior, Institute of Geochemistry, Chinese Academy of Sciences, Guiyang, Guizhou 550081, China

<sup>2</sup>University of Chinese Academy of Sciences, Beijing 100039, China

<sup>a)</sup>Author to whom correspondence should be addressed: [dailidong@gyig.ac.cn](mailto:dailidong@gyig.ac.cn).

## ABSTRACT

High-pressure phase stability of gallium phosphide was explored under different hydrostatic environments up to 40.0 GPa in a diamond anvil cell. Two irreversible phase transitions from the semiconductor to metal to an amorphous state appear at 19.8 and 31.5 GPa and as well as 22.6 and 35.3 GPa under nonhydrostatic and hydrostatic environments, respectively. Furthermore, the hysteresis effect of the high-pressure phase transition of a sphalerite-structure compound under a hydrostatic environment was disclosed. All of the obtained results can provide new insight into the underlying structural evolution and electrical transport characteristics for the semiconducting compound at different hydrostatic environments.

Published under license by AIP Publishing. <https://doi.org/10.1063/1.5093949>

As we know, the degree of hydrostaticity in the sample chamber of a diamond anvil cell plays a crucial role in turning the physicochemical properties of a semiconducting compound under high pressure, especially for the sphalerite-structure compound (e.g., ZnSe and ZnTe).<sup>1,2</sup> Recently, some previous high-pressure Raman scattering and electrical conductivity results on the sphalerite-structure compound have confirmed that the degree of hydrostaticity has a significant impact on the pressure point and reversibility of the structural phase transition, metallization, and amorphization. For instance, the occurrence of structural phase transition and metallization for zinc selenide (ZnSe) with the sphalerite structure has been proven to be sensitive to different hydrostatic environments. Compared with the nonhydrostatic environment, one available ~2.0 GPa hysteresis effect of phase transition pressure for ZnSe is confirmed under the hydrostatic condition. The reversible metallization phase transformation of ZnSe appears only at the hydrostatic environment.<sup>1</sup>

High-pressure characterizations for the cubic sphalerite-structure semiconducting compounds have attracted tremendous interest for their widespread application in the field of electronic and optoelectronic materials.<sup>3,4</sup> As a representative cubic sphalerite-structure compound, GaP crystallizes in the face-centered cubic structure with the  $F-43m$  space group at ambient conditions. Owing to the principal raw material in the product of a complex light-emitting diode for GaP, its physical and chemical properties have received more and more attention. However, until now, it remains unclear that the degree of hydrostaticity affects the high-pressure physical properties for GaP. Therefore, it is crucial to systematically reveal the high-pressure behavior of GaP under different hydrostatic environments.

All of the high-pressure experiments were conducted in the diamond anvil cell with an anvil culet of 300  $\mu\text{m}$  in diameter. The pressure medium (PM) of liquid helium was selected to obtain a hydrostatic environment, and no pressure medium was used for the

nonhydrostatic condition. As shown in Fig. 1, the present designed DAC assemblage for the high-pressure electrical conductivity measurement is composed of two symmetric blocks with the oriented column, the hexagonal socket screw, the diamond anvil, the rhenium gasket, and the molybdenum metallic electrode. Pressure calibration was conducted by the wavenumber shift of the fluorescence band of the trivalent chromic ion of a ruby single crystal.<sup>5</sup> In order to obtain the deviatoric stress of the sample under the nonhydrostatic environment, several small ruby spheres were added in the center and at the edge of the sample chamber. The inset of Fig. 2 shows that the deviatoric stress in the sample chamber nonlinearly increased with pressure. For the HRTEM and AFM measurements, the GaP powder sample was first compressed up to the designated maximum pressure point in the diamond anvil cell. Upon decompression, the recovered sample was dissolved in the deionized water and fully stirred. Then, the solution was transferred into the lacey support film and the glass substrate by using a micropipettor for the HRTEM and AFM measurements, respectively. The sample was kept for the natural drying in the superclean laboratory.

Representative results on the variations of Raman peaks and corresponding Raman shifts of GaP are displayed in Fig. 2 under the nonhydrostatic environment. At 0.5 GPa, there appeared two typically characteristic peaks at 363.3 and 400.6 cm<sup>-1</sup> corresponding to the transverse optical (TO) and longitudinal optical (LO) phonons of the sample, respectively, which was in good agreement with previous studies at ambient conditions.<sup>6,7</sup> Two discontinuities for TO and LO modes at ~19.8 GPa are possibly related to the phase transition from the cubic sphalerite to orthorhombic (Cmcm) phase. At pressure beyond 31.5 GPa, only one broad hump was observed, which indicated the occurrence of a crystalline-to-amorphous transformation for GaP. As for the hydrostatic environment, a similar structural phase transition and amorphization for GaP were determined at the respective pressures of 22.6 and 35.3 GPa (Fig. S1). The unrecovered Raman spectra suggest that the phase transition of amorphization was irreversible under both nonhydrostatic and hydrostatic conditions. The fitted parameters on the variations of LO and TO modes under different hydrostatic environments are detailedly listed in Table I (the supplementary material).

Typical impedance spectra and the fitted electrical conductivity for GaP with pressure are displayed in Fig. 3 at atmospheric temperature. At 20.1 GPa, the logarithmic electrical conductivity of GaP exhibits a drastically discontinuous increase from approximately -5.5 to -1.2 S cm<sup>-1</sup>. At pressures above 20.1 GPa, the relatively stable and high conductivity values for GaP may be

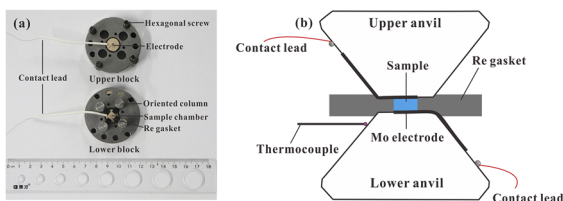


FIG. 1. (a) Experimental setup of GaP for high-pressure electrical conductivity measurements. (b) Schematic view of the DAC for high-pressure conductivity experiments.

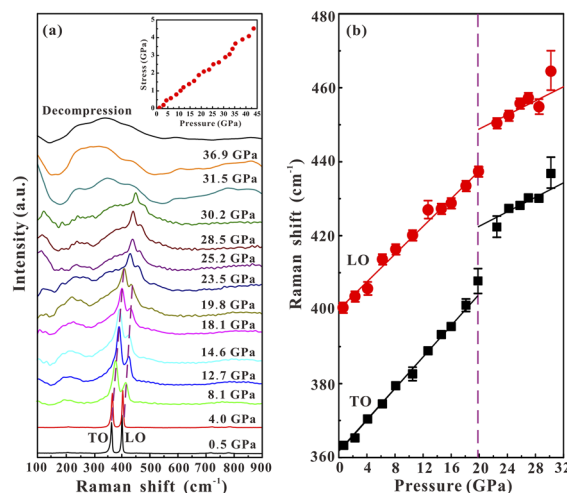


FIG. 2. (a) Raman spectroscopic results of GaP at the elevated pressures under the nonhydrostatic environment. (b) The Raman shift of two typical vibrational modes with increasing pressure. Inset: The deviatoric stress of the sample at the pressure range of 1.1–43.6 GPa. TO: transverse optical mode and LO: longitudinal optical mode.

attributed to a semiconductor-to-metal transformation. Furthermore, the phase transition of metallization was confirmed by a series of high-pressure variable temperature conductivity measurements (Fig. S2). In light of the dependence of electrical conductivity on

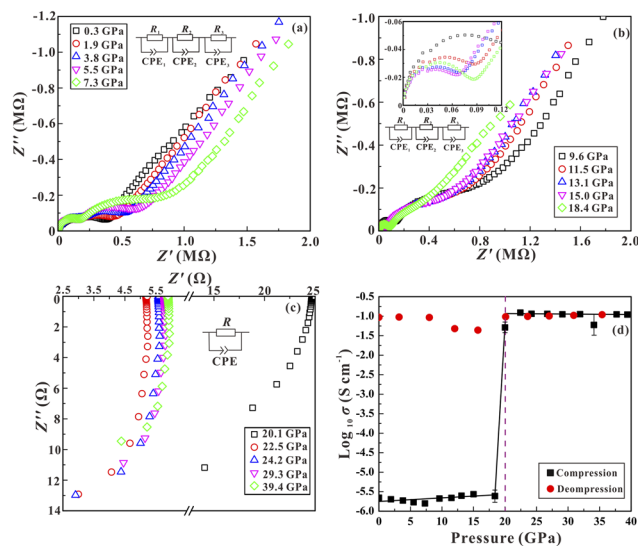
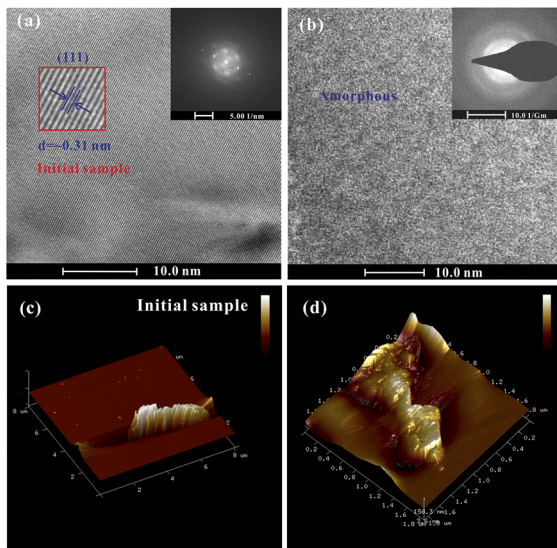


FIG. 3. [(a)–(c)] Complex impedance spectra of GaP at the pressure range of 0.3–39.4 GPa. The equivalent circuit of (a) and (b) that is composed of the series connection of  $R_1$ -CPE<sub>1</sub>,  $R_2$ -CPE<sub>2</sub>, and  $R_3$ -CPE<sub>3</sub> is selected to model the impedance spectra. The equivalent circuit of (c) is taken as a simple R-CPE circuit. (d) The pressure dependence of logarithm of electrical conductivity for GaP. R: resistance and CPE: constant phase element.



**FIG. 4.** HRTEM images of (a) the initial GaP and (b) the decompressed GaP sample from 36.9 GPa under the nonhydrostatic environment. Inset: Representative cross-sectional selected-area electron diffraction patterns by HRTEM. AFM images of (c) the initial GaP and (d) the decompressed GaP from 37.4 GPa under the nonhydrostatic environment. PM: pressure medium.

temperature from positive to negative interrelation, the metallization points were determined at respective 20.2 and 22.3 GPa under nonhydrostatic and hydrostatic environments. The metallic characteristics of GaP always remain up to the designated experimental maximum pressure point of 37.2 GPa. The calculated activation energy gradually decreases with pressure (Fig. S3). At  $\sim 20.0$  GPa, the magnitude of activation energy approaches zero, which indicated the occurrence of the pressure-induced metallization. In the comprehensive consideration with the above-obtained Raman scattering results, we can conclude that the electronic semiconductor to metal transition for GaP is associated with a structural transition from the sphalerite to Cmc $m$ -type phase at  $\sim 20.0$  GPa. As for the amorphous state at  $\sim 31.0$  GPa, the electronic structure of the sample did not change, which is characterized by a metallic behavior.

From the HRTEM microscopic observation and the corresponding selected area electron diffraction pattern (SAED) images for the initial GaP in Fig. 4(a), the interlayer spacing along the orientation of (111) plane is estimated as  $\sim 0.31$  nm with a series of highly ordered crystalline structural spots. Upon decompression, the adjacent layer boundary became rather blurry with the relatively dim single ring caused by some randomly scattered electrons under the nonhydrostatic environment, which revealed a dominant amorphous state in the recovered GaP [Fig. 4(b)]. As shown in Figs. 4(c)

and 4(d), the AFM morphology images of the recovered samples are characterized by a completely distinguishable to lumpy surface layer. It makes clear that the original surface structure of the initial GaP was thoroughly destroyed upon compression. As for the hydrostatic environment, the HRTEM and AFM images also disclosed an amorphous phase in the recovered samples, as shown in Fig. S4. In brief, all of these obtained results from HRTEM and AFM images exhibited the pressure-induced irreversible crystalline-to-amorphous phase transition for GaP under both nonhydrostatic and hydrostatic environments.

In summary, the hysteresis effect in the pressure points from the semiconductor to metal to amorphous state of GaP at the hydrostatic environment has been revealed, which indicated that the pressure medium of liquid helium played a vital role in the protection of the crystalline structure. Due to the existence of the pressure medium, the hydrostatic environment of the sample chamber is capable of relieving the deviatoric stress in the diamond anvil cell and resulting in the hysteresis effect of metallization and amorphization for GaP. In conclusion, it is crucial to fully consider the degree of hydrostaticity for deeply fascinating insights into the structural phase transition, metallization, and amorphization for the semiconducting material under high pressure.

See [supplementary material](#) for the complete Raman spectra, pressure-dependent variable temperature electrical conductivity results, pressure dependence of the activation energy, and HRTEM and AFM images of GaP under the hydrostatic condition.

This research was financially supported by the Strategic Priority Research Program (B) of the Chinese Academy of Sciences (No. 18010401), the Key Research Program of Frontier Sciences of CAS (No. QYZDB-SSW-DQC009), the Hundred Talents Program of CAS, the NSF of China (Grant Nos. 41774099 and 41772042), the Youth Innovation Promotion Association of CAS (No. 2019390), the Special Fund of the West Light Foundation of CAS, and the Postdoctoral Science Foundation of China (No. 2018M643532).

## REFERENCES

- <sup>1</sup>C. Pu, L. D. Dai, H. P. Li, H. Y. Hu, K. X. Liu, L. F. Yang, and M. L. Hong, *AIP Adv.* **9**, 025004 (2019).
- <sup>2</sup>Y. K. Zhuang, L. D. Dai, H. P. Li, H. Y. Hu, K. X. Liu, L. F. Yang, C. Pu, and M. L. Hong, *Mod. Phys. Lett. B* **32**, 1850342 (2018).
- <sup>3</sup>A. R. Aparna, V. Brahmajirao, and T. V. Karthikeyan, *Procedia Mater. Sci.* **6**, 1650 (2014).
- <sup>4</sup>L. Lin, G. T. Woods, and T. A. Callcott, *Phys. Rev. B* **63**, 235107 (2001).
- <sup>5</sup>H. K. Mao, J. Xu, and P. M. Bell, *J. Geophys. Res.: Solid Earth* **91**, 4673, <https://doi.org/10.1029/jb091ib05p04673> (1986).
- <sup>6</sup>M. P. Jackson, M. P. Halsall, M. Gungerich, P. J. Klar, W. Heimbrot, and J. F. Geisz, *Phys. Status Solidi B* **244**, 336 (2007).
- <sup>7</sup>R. Aggarwal, A. A. Ingale, and V. K. Dixit, *Appl. Surf. Sci.* **427**, 754 (2018).